

Seismic fragility evaluation of arch concrete dams through nonlinear incremental analysis using smeared crack model

JavadMoradloo*, Kiarash Naserasadi^a and Habib Zamani^b

Department of Civil Engineering, School of Engineering, University of Zanjan, Zanjan, Iran

(Received April 24, 2017, Revised July 18, 2018, Accepted July 21, 2018)

Abstract. In the present study, a methodology for developing fragilities of arch concrete dams to assess their performance against seismic hazards is introduced. Firstly, the probability risk and fragility curves are presented, followed by implementation and representation of the way this method is used. Amirkabir arch concrete dam was subjected to non-linear dynamic analyses. A modified three dimensional rotating smeared crack model was used to take the nonlinear behavior of mass concrete into account. The proposed model considers major characteristics of mass concrete. These characteristics are pre-softening behavior, softening initiation criteria, fracture energy conservation, suitable damping mechanism and strain rate effect. In the present analysis, complete fluid-structure interaction is included to account for appropriate fluid compressibility and absorptive reservoir boundary conditions. In this study, the Amirkabir arch concrete dam is subjected to a set of 8 three-component earthquakes each scaled to 10 increasing intensity levels. Using proposed nonlinear smeared crack model, nonlinear analysis is performed where the structure is subjected to a large set of scaled and un-scaled ground motions and the maximum responses are extracted for each one and plotted. Based on the results, fragility curves were plotted according to various and possible damages indexes. Discrete damage probabilities were calculated using statistical methods for each considered performance level and incremental nonlinear analysis. Then, fragility curves were constructed based on the lognormal distribution assumption. Two damage indexes were introduced and compared to one another. The results indicate that the dam has a proper stability under earthquake conditions at MCE level. Moreover, displacement damages index is more conservative and impractical in the fragility analysis than tensional damage index.

Keywords: seismic fragility analysis; arch concrete dam; non-linear analysis; smeared crack model

1. Introduction

The seismic behavior of concrete dams subjected to earthquake loading cannot be accurately evaluated by only a nonlinear dynamic analysis. The results of such an analysis for concrete dams depend on such different factors as earthquake records, dam and foundation materials, interaction effects, reservoir depth and other factors. So, in evaluation of dam safety, we need to take a lot of uncertain factors into account. In addition to a nonlinear analysis, a probability analysis on dam safety seems to be necessary. Seismic fragility curve is a probabilistic damage analysis method which shows the effect of uncertainty on results.

The fragility curves have been previously extracted in the studies of power plant tanks, steel and concrete frames and bridges, but these curves are newly employed for concrete dams, and especially arch concrete dams. Ellingwood, and Tekie (2001) evaluated fragility curves for Bluestone gravity concrete dam. They extracted the curves

for 12 different earthquake records, and evaluated the uncertain effects such as the interaction ratio of pressure and friction between the dam and its foundation on these curves. They used concrete damage in dam neck, foundation around the dam toe, foundation and dam sliding, and crown to toe displacement as four damage indexes. Lin and John (2008) evaluated the seismic vulnerability of concrete gravity dams, earth fill dams and rock fill dams in Canada according to their fragility curves. The most obvious results obtained from the curves were showed that for an equivalent seismic movement, earth fill and rock fill dams have a higher vulnerability probability than concrete gravity dams. Ghaemian and Mirzahassein Kashani (2008) conducted a fragility analysis using nonlinear analyses on Pine Flat concrete gravity dam. They used six near field earthquake records and two foundation models (mass-less and massive). They employed the log normal statistical distribution to extract fragility curves. The crack lengths between the foundation and dam base and the total area of the cracked elements in the dam body were selected as damage indexes. The results of the study indicated that the probability of the first structural limiting state-i.e., the limitation of the crack length at the base of the dam-was about 23% in mass-less foundation model and in a massed one it was 10%. When using the second structural limiting state-i.e., the area of cracked elements in the dam body-the probabilities of the second structural limiting state in the model with a mass-less foundation and a massed foundation

*Corresponding author, Ph.D.

E-mail: ajmoradloo@znu.ac.ir

^aPh.D.

E-mail: Naserasadi@znu.ac.ir

^bM.Sc. Graduated

E-mail: Zamani.habaib@yahoo.com

model are closer to one another. Kang and Lee (2016) proposed a new structural damage index for seismic fragility analysis of reinforced concrete columns. The proposed damage index is formulated based on the nonlinear regression of experimental column test data. Mehan *et al.* (2013) presented the assessment of seismic fragility curves for reinforced concrete buildings. Analytical seismic fragility curves for RC buildings were determined based on post-earthquake survey. The information about the damaged RC buildings was investigated and evaluated by experts. Using the field observed damage data, the Japanese Seismic Index Methodology, and the capacity design method, seismic fragility curves were developed for those buildings. Karim and Yamazak (2001) are the pioneers of presenting fragility curves for bridges. They assumed the bridge column as a free one degree system and evaluated the effect of two accelerations from two different codes. The analytical fragility curves were compared with the empirical ones. The empirical fragility curves cannot introduce various structural parameters and characteristics of input motion, and they require a large amount of actual damage data for a certain class of structures. Hence, the analytical method employed in this study may be used in constructing the fragility curves for a class of bridge structures, which are not affected by earthquake so often. The results showed that the damage probabilities for both codes were nearly equal and the damage probabilities for codes were more than that of 1998 earthquake in Japan. Shinozuka *et al.* (2007) improved the fragility curves for multi-span reinforced concrete bridges. They used time history dynamic analyses in their research and fragility curves were produced based on two assumptions: 1) bridge was symmetric and all the piers were located on the same soil type 2) the soil under the piers was not homogenous. The fragility curves were improved by altering the soil type under the bridge piers. This report integrates statistical and analytical methods for the seismic performance evaluation of highway transportation networks. In this report, the application of fragility curves in the performance-based design of bridges was demonstrated. The design-acceptance criteria were suggested that verified the target performance of a newly designed bridge under a prescribed level of seismic hazard. Borekci and Kircil (2011) investigated fragility of R/C frame buildings. They considered different types of hysteretic models. Discrete damage probabilities were calculated using elastic spectral displacement. Furthermore, the effect of hysteresis model parameters on the damage probability was investigated. Last but not least, Jovanoska (2000) obtained the fragility curves for reinforced concrete structures. As a result of the analytical research, the values of the global damage index were determined. Using the data from the nonlinear dynamic analyses, the two sets of fragility curves and damage probability matrices were defined. Kadkhodayana *et al.* (2015) applied IDA approach to analyze a thin high arch dam. The parameters of S_a , PGA and PGV were used as intensity measures and the overstressed area was utilized as engineering demand parameter. Then, three limit states were assigned to the considered structure using the IDA curves. Subsequently, fragility curves were calculated. It

was showed that the PGA is a better parameter to measure intensity. Moreover, it was found that-utilizing the proposed methodology-quantifying the qualitative limit states is possible. Hariri-Ardebili and Saouma (2016) presented the probabilistic seismic demand model (PSDM) which demonstrated the relationship between the intensity and the engineering demand parameter (EDP) (such as displacement and crack ratio-ratio of crack length to total crack pat). Then, cloud analysis is performed where the structure is subjected to a large set of un-scaled ground motions and the maximum responses were extracted for each one and plotted as a cloud of results. When the results of the cloud analysis were aggregated, it became possible to plot the seismic fragility curve which was the probability of EDP exceedance in terms of the IM parameter. Alembagheri and Ghaemian (2013) presented seismic damage of concrete arch dams by applying the Incremental Dynamic Analysis method. The performance and various limit-states of the structure are evaluated and simple damage indices were proposed through comparison of response demands in earthquake analysis with the determined structural capacities. It was found that the proposed damage indices can properly indicate state of damage in the dam body. Pekau *et al.* (1991) used a model, based on linear elastic fracture mechanics theory, to simulate the nonlinear behavior of gravity dams. The boundary element method was used to discretize dam and reservoir domain. It was concluded that procedures proposed to simulate the impact effect of crack-closing predicted complete penetration of the crack through the upper part of the dam, which is consistent with the observed prototype behavior. Feng and Pekau (1996) investigated cracking of gravity dams using linear elastic fracture mechanics and boundary element method. The Kolnbrein arch dam was considered for case study. It was also noted that the bonded condition at the interface between the dam and the upstream elevated foundation was responsible for producing the distinctive profile of the observed crack, which daylight on the upstream face at an acute angle. Al-Eidi and Hall's (1996a, b) studies were probably the first to employ nonlinear fracture mechanics to simulate concrete dam behavior. The considered nonlinear behaviors involved concrete cracking and fluid cavitations in the reservoir. The pore pressure was considered in the cracks. The results showed that cavitation had a negligible effect on the dam response, while cracking was significant in dam response. Gunglun *et al.* (2000) proposed a smeared crack model based on bezant's crack band theory. Furthermore, a technique of finite element re-mesh was presented for a better accommodation of the crack extension. In addition, several features of the present analysis, influencing the predicted concrete fracture process, were also studied. Battacharjee and Leger (1992) used a smeared crack model to conduct a seismic analyze of concrete gravity dams. A review of the past finite element seismic fracture analyses of concrete gravity dams reveals that reliable numerical models for safety evaluation of the structures during severe ground motions have not been satisfactorily developed yet. Ghrib and Tinawi (1995) proposed a new model based on continuum damage mechanics for seismic fracture analysis of gravity dam.

Only one damage variable was considered for tensional damage. A constitutive model for plain concrete, subjected to tensile stresses, was presented. The mesh-dependent hardening technique was adopted so that the fracture energy dissipation could not be affected by size of the finite element mesh. The results confirmed the importance of accounting for the initial state for the seismic safety evaluation of an existing dam. Faria *et al.* (1998) proposed a 3-dimensional damage mechanics model for analysis of gravity and arch concrete dam. Concrete was modeled by an isotropic model that capable of incorporating tensional and compression damage. The efficiency of numerical predictions made by the constitutive model was illustrated through numerical applications. Among the possible outputs from the model, the structural distributions of both tensile and compressive damage variables provided helpful tools for the identification of the most affected concrete domains. Mizabozorb (2005) used a three dimensional damage mechanics model to investigate nonlinear behavior of concrete arch dam. Morrow Point dam was analyzed in a case study to consider its nonlinear seismic behavior. The deduced results showed that the resulting crack profiles were in good agreement with the contour of maximum principal stresses and no numerical instability occurred during the analysis. Oudni and Bouafia (2015) investigated the earthquake damage response of the concrete gravity dams. The proposed damage model took the dissymmetry of the behavior of concrete, cracking in tension, and rupture in compression into account. Two dimensional seismic analysis of Koyna gravity dam was presented using the 1967's Koyna earthquake records. The results were shown on the time history graphs of the horizontal and vertical displacements in the crest of the dam. Hariri-Ardebili *et al.* (2013) proposed an improved 3D co-axial rotating smeared crack model with the ability of updating the variable shear transfer coefficient. It was found that the proposed model led to less diffused cracks in concrete dams and matched reasonably with the results obtained from experimental tests. Omidi *et al.* (2013) utilized two different damping mechanisms to examine the seismic cracking response of concrete gravity dams by a plastic-damage model. It was concluded that employing the damage-dependent damping mechanism led to more extensive damages and also predicted more reliable crack patterns than the constant damping mechanism in seismic analysis of concrete dams. Lu *et al.* (2016) proposed a three-dimensional elastoplastic constitutive model for concrete using hardening and softening functions which were determined from the uniaxial compressive stress-strain relationship. The simulations showed that the proposed constitutive model was able to describe the nonlinear mechanical behavior under complex stress states with high computational efficiency.

In the upcoming sections of this paper, the basic concepts and employed models will be briefly explained. In the present study, a modified three-dimensional smeared crack model was used to take the nonlinear behavior of mass concrete into account. The proposed model considered major characteristics of mass concrete under three-dimensional loading conditions. These characteristics were

pre-softening behavior, softening initiation criteria, fracture energy conservation, suitable damping mechanism and strain rate effect. After model verification, the nonlinear dynamic analysis of Amirkabir arch concrete dam was carried out and seismic fragility curves was extracted, based on deduced results and proposed models. Finally, safety evaluation of dam was presented, based on the fragility curves. Seismic fragility curves were plotted according to various and possible damages for arch concrete dams. Two damage indexes were introduced and compared to one another. The deduced results showed that displacement damages index was a more conservative and impractical index in the fragility analysis compared to tensional damage index.

2. Basic concepts and methodology

2.1 Proposed crack model

A comprehensive numerical model in fracture mechanics analysis of mass concrete should be able to simulate the behavior of concrete in three different conditions: Pre-softening, softening and crack closing/reopening. Based on previous studies, a reliable smeared crack model must possess some minor but important components such as: softening initiation criteria, fracture energy conservation, damping mechanism for cracked element, characteristic length and dynamic magnification factors for concrete parameters.

2.1.1 Pre-softening behavior modeling

In this study, linear elastic behavior is considered at the pre-softening stage of mass concrete.

2.1.2 Softening initiation criterion

The uniaxial strain energy has been used as the softening initiation criterion. This criterion considers the effects of other components of stress and strain and it is successfully used in the static and dynamic analysis of concrete dams (Moradloo 2007, Omidin *et al.* 2013, Harir *et al.* 2013, Mirzabozorg 2005, Gunglun *et al.* 2000). Based on this criterion, the crack initiates when the uniaxial strain energy density is greater than material parameter

$$U > U_0 \quad (1)$$

Where U is uniaxial strain energy density and equals to

$$U = \frac{1}{2} \sigma_1 \varepsilon_1 \quad (2)$$

σ_1, ε_1 are the first principal stress and strain of an integration point, respectively. U_0 is material parameter and equals to

$$U_0 = \frac{1}{2} \sigma_0 \varepsilon_0 \quad (3)$$

Where σ_0, ε_0 are the apparent tensile strength and its corresponding strain, respectively. Since the pre-peak stress-strain relationship is assumed to be linear, the apparent tensile strength is calibrated in such a way that a linear elastic uniaxial stress-strain relationship up to σ_0 will

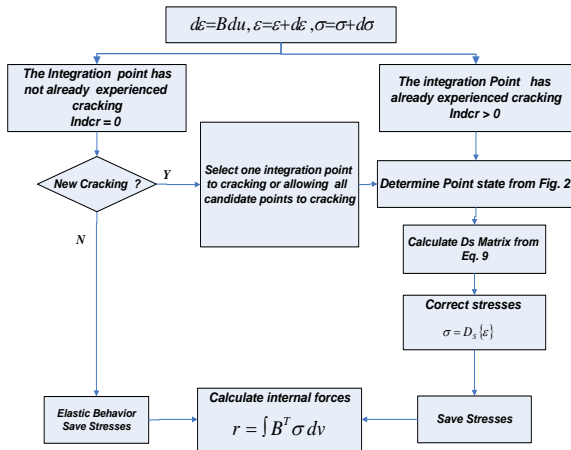


Fig. 1 Stress, stiffness matrix and internal forces calculation algorithm

preserve the value of U_0 . The above relations are valid under static loading conditions. For dynamic loading, material parameter is multiplied by a dynamic magnification factor DMF_t .

2.1.3 Softening behavior

After Crack initiation, the isotropic constitutive matrix is replaced with an orthotropic constitutive matrix, while their components are determined by stiffness degradation levels corresponding to three principal direction stresses. In present study, the SMS (Secant Module Stiffness) approach is employed to formulate stiffness in which the constitutive relation is defined in terms of total stress and strain. Based on SMS formulation, the total strains on crack plane $\{\Delta\varepsilon\}$ is decomposed into elastic $\{\Delta\varepsilon^{co}\}$ and cracking $\{\Delta\varepsilon^{cr}\}$ components

$$\{\Delta\varepsilon\} = \{\Delta\varepsilon^{co}\} + \{\Delta\varepsilon^{cr}\} \quad (4)$$

The superscript ‘co’ corresponds to the elastic components of total strain and superscript ‘cr’ corresponds to cracked portion of total strain. The cracked strain is related to the corresponding cracked stress using the cracked constitutive matrix $[D^{cr}]$ as follows

$$\{\sigma^{cr}\} = [D^{cr}]^T \{\varepsilon^{cr}\} \quad (5)$$

After some algebraic operations cracked constitutive matrix $[D_s]$ in the global coordinates system is given based on Moradloo (2007), Harir *et al.* (2013), Mirzabozorg (2005)

$$[D_s] = [D^{co}] - [D^{co}][T][D^{cr}] + [T]^T [D^{co}][T]^{-1} [T]^T [D^{co}] \quad (6)$$

Where $[D^{co}]$ is the intact module matrix and $[T]$ is the transformation matrix which transforms the vector of cracked strain to the global coordinate direction. This matrix in rotating crack model (RCM) is changed in every iteration, but in fixed crack model (FCM) it is constant after first crack initiation. In a special case, where normal crack plane is parallel to the global x direction and the two other tangential local directions are parallel to the other global directions, the total secant matrix in local co-ordinates is given as

$$[D]_{nst} = \begin{bmatrix} D_{11} & D_{12} & D_{13} & 0 & 0 & 0 \\ D_{21} & D_{22} & D_{23} & 0 & 0 & 0 \\ D_{31} & D_{32} & D_{33} & 0 & 0 & 0 \\ 0 & 0 & 0 & D_{44} & 0 & 0 \\ 0 & 0 & 0 & 0 & D_{55} & 0 \\ 0 & 0 & 0 & 0 & 0 & D_{66} \end{bmatrix} \quad (7)$$

Where

$$D_{11} = \frac{\eta_1 E (1 - \nu^2 \eta_2 \eta_3)}{1 - \nu^2 \eta_1 \eta_2 - \nu^2 \eta_3 \eta_2 - \nu^2 \eta_1 \eta_3 - 2\nu^3 \eta_1 \eta_2 \eta_3},$$

$$D_{22} = \frac{\eta_2 E (1 - \nu^2 \eta_1 \eta_3)}{1 - \nu^2 \eta_1 \eta_2 - \nu^2 \eta_3 \eta_2 - \nu^2 \eta_1 \eta_3 - 2\nu^3 \eta_1 \eta_2 \eta_3}$$

$$D_{33} = \frac{\eta_3 E (1 - \nu^2 \eta_2 \eta_1)}{1 - \nu^2 \eta_1 \eta_2 - \nu^2 \eta_3 \eta_2 - \nu^2 \eta_1 \eta_3 - 2\nu^3 \eta_1 \eta_2 \eta_3},$$

$$D_{12} = \frac{\nu \eta_1 \eta_2 E (1 + \nu \eta_3)}{1 - \nu^2 \eta_1 \eta_2 - \nu^2 \eta_3 \eta_2 - \nu^2 \eta_1 \eta_3 - 2\nu^3 \eta_1 \eta_2 \eta_3} \quad (8)$$

$$D_{23} = \frac{\nu \eta_3 \eta_2 E (1 + \nu \eta_1)}{1 - \nu^2 \eta_1 \eta_2 - \nu^2 \eta_3 \eta_2 - \nu^2 \eta_1 \eta_3 - 2\nu^3 \eta_1 \eta_2 \eta_3},$$

$$D_{13} = \frac{\nu \eta_1 \eta_3 E (1 + \nu \eta_2)}{1 - \nu^2 \eta_1 \eta_2 - \nu^2 \eta_3 \eta_2 - \nu^2 \eta_1 \eta_3 - 2\nu^3 \eta_1 \eta_2 \eta_3}$$

$$D_{44} = \beta_{12} G, \quad D_{55} = \beta_{23} G, \quad D_{66} = \beta_{13} G$$

$$\eta_i = \frac{E_i^s}{E}$$

The constitutive matrix in global coordinate system can be obtained as follows

$$[D]_s = [T]^T [D]_{nst} [T] \quad (9)$$

Matrix $[T]$ was introduced earlier. Based on the maximum strain reached in each principal direction, the secant module matrix is determined as shown in figure 1. Increasing the normal strain in each direction leads to reduction of corresponding softened young’s modules. Finally, when the maximum strain reaches the fracture strain, integration point in the corresponding direction is fully cracked and the softened young modules are set at zero.

In above equations, β_{ij} are shear retention factors. In the earliest three-dimensional smeared crack models, it was assumed that the softened shear module in two tangential directions was zero. In some situations, it could lead to numerical problems. Some of the scholars assumed various empirical descending relations for shear module versus normal strain. In the proposed formulation, based on the concept of co-axially of fracture plane and principal stress, shear retention factors can be calculated easily

$$G_s = \frac{\sigma_1 - \sigma_2}{2(\varepsilon_1 - \varepsilon_2)} \quad (10)$$

Where G_s is the softened shear module corresponding to i-j axes on the fracture plane and σ_i, ε_i are principal stresses

and strains corresponding to the principal directions of j and k . Using Eqs. (7) and (10), the stress-strain relationship in three-dimensional space is given as follows

$$\begin{aligned}\varepsilon_n &= \frac{1}{E\eta_1}(\sigma_n - \nu\eta_1\sigma_s - \nu\eta_1\sigma_t), \\ \varepsilon_s &= \frac{1}{E\eta_2}(\sigma_s - \nu\eta_2\sigma_n - \nu\eta_2\sigma_t), \\ \varepsilon_t &= \frac{1}{E\eta_3}(\sigma_t - \nu\eta_3\sigma_n - \nu\eta_3\sigma_s)\end{aligned}\quad (11)$$

Combining Eqs. (10) and (11), the shear retention factors in Eq. (7) are determined as follows

$$\begin{aligned}\beta_{12} &= \frac{1+\nu}{1-\nu^2\eta_1\eta_2 - \nu^2\eta_3\eta_2 - \nu^2\eta_1\eta_3 - 2\nu^3\eta_1\eta_2\eta_3} \left(\frac{\eta_1\varepsilon_1 - \eta_2\varepsilon_2}{\varepsilon_1 - \varepsilon_2} + \frac{\nu\eta_1(\eta_1 - \eta_2)\varepsilon_3}{\varepsilon_1 - \varepsilon_2} - \nu\eta_1\eta_2 - 2\nu^2\eta_1\eta_2\eta_3 \right) \\ \beta_{23} &= \frac{1+\nu}{1-\nu^2\eta_1\eta_2 - \nu^2\eta_3\eta_2 - \nu^2\eta_1\eta_3 - 2\nu^3\eta_1\eta_2\eta_3} \left(\frac{\eta_2\varepsilon_2 - \eta_3\varepsilon_3}{\varepsilon_2 - \varepsilon_3} + \frac{\nu\eta_2(\eta_2 - \eta_3)\varepsilon_1}{\varepsilon_2 - \varepsilon_3} - \nu\eta_1\eta_3 - 2\nu^2\eta_1\eta_2\eta_3 \right) \\ \beta_{13} &= \frac{1+\nu}{1-\nu^2\eta_1\eta_2 - \nu^2\eta_3\eta_2 - \nu^2\eta_1\eta_3 - 2\nu^3\eta_1\eta_2\eta_3} \left(\frac{\eta_1\varepsilon_1 - \eta_3\varepsilon_3}{\varepsilon_1 - \varepsilon_3} + \frac{\nu\eta_1(\eta_1 - \eta_3)\varepsilon_2}{\varepsilon_1 - \varepsilon_3} - \nu\eta_1\eta_3 - 2\nu^2\eta_1\eta_2\eta_3 \right)\end{aligned}\quad (12)$$

2.1.4 Crack closing/reopening behavior

Various models are proposed to model loading/unloading in smeared crack approach (Moradloo 2007, Hariri *et al.* 2013, Mirzabozorg 2005, Gunglun *et al.* 2000). In the present study, the closing/reopening criterion is based on value of the principal strains. It has been shown that under cyclic loads there is residual strain in the closed crack. Based on this concept, the total strain can be decomposed into two components of recoverable elastic and residual strain given as

$$\varepsilon = \varepsilon^e + \varepsilon^{res} = \varepsilon^e + \lambda\varepsilon_{max}\quad (13)$$

Where ε_{max} is the maximum principal strain that point has experienced during the previous loading and λ is the ratio between residual strain in the closed crack and the maximum principal strain and is usually assumed to be 0.2.

2.1.5 Damping mechanism for cracked element

It has been shown that conventional Rayleigh damping model could lead to numerical problems in seismic crack analysis. It is mainly evident from mass proportional component of damping. In the present study, the Elasto-Brittle Damping (EDM) and Linear Damping models (LDM) are employed. In EDM model, damping of cracked point equals zero, and in LDM model damping of cracked point is proportional to current stiffness of material.

2.1.6 Characteristic length

In the present study, it is assumed that the mesh size property- measured by the characteristic length- is equal to the cubic root of volume affected by integration point as

$$h_c = \sqrt[3]{w_i w_j w_k \det J}\quad (14)$$

2.1.7 Fracture energy conservation

Fracture energy conservation is preserved once the following fracture strain is used

$$\varepsilon_f = \frac{2G_f}{h_c f_t}\quad (15)$$

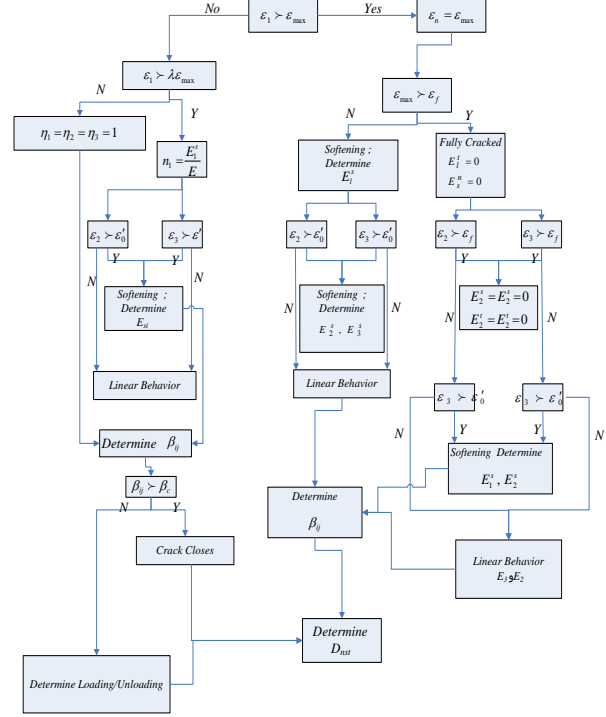


Fig. 2 The proposed algorithm for state determination of integration point

Where: ε_f , G_f , h_c , f_t are ultimate uniaxial strain, fracture energy, characteristic length and uniaxial tensile strength, respectively. In dynamic loading, material parameters are magnified by related dynamic magnification factors.

2.1.6 Dynamic magnification factors for concrete parameters

It is shown that material parameters of concrete in dynamic loading are different from static values. It mainly originates from fact that in dynamic loading crack passes across aggregate and because of its strength, module of elasticity and fracture toughness will increase. A few studies were carried out based on viscoelastic models to consider strain rate effects on concrete behavior (Faria *et al.* 1998, Omidi *et al.* 2013). In the present study, strain rate effects are modeled by proper dynamic magnification factors. In this way, dynamic material parameters are given as

$$\begin{aligned}G'_f &= DMF_g G_f, \quad f'_t = DMF_t f_t, \\ E' &= DMF_e E\end{aligned}\quad (16)$$

Where primed parameters relate to dynamic values.

2.1.7 Proposed crack algorithm

In the present paper, a rotating smeared crack model, based on above relations, is presented. Cracking is considered in integration points. The implementation of the proposed smeared crack constitutive model is illustrated by Figs. 1 and 2 which show all the operations needed to evaluate the stiffness matrix, residual internal forces and state of integration points. Fig. 1 represents the calculation of stiffness matrix and internal forces. Crack state determination flowchart is presented in Fig. 2.

2.2 Fluid structure interaction

The governing equation for fluid domain is the Helmholtz equation for hydrodynamic pressure

$$\nabla^2 P = \frac{1}{C^2} \ddot{P} \quad (17)$$

Where P , C are the hydrodynamic pressure and the acoustic wave velocity in water, respectively. The above equation implies small displacements of inviscid compressible fluid with an irrotational motion. Water compressibility has a significant influence on the fluid-structure interaction for a wide range of ratio of natural frequencies of structure to fluid domain, including the case of higher and stiffer dams (Ghaemian *et al.* 1998). Thus, for general applicability and completeness of the dam-reservoir formulation, one needs to include the reservoir water compressibility.

Boundary conditions for Helmholtz equation in a concrete dam-reservoir interaction problem are expressed as

$$\left[\frac{\partial P}{\partial y} + \frac{1}{g} \ddot{P} \right]_{y=\eta} = 0 \quad (18)$$

That is called Cauchy Boundary Condition for the reservoir-free surface,

$$\frac{\partial P}{\partial n} = -\rho \ddot{a}_{gn} - \frac{1}{\beta C} \frac{\partial P}{\partial t} \quad (19)$$

For the reservoir bottom partial absorption and normal component of earthquake records

$$\frac{\partial P}{\partial x} = -\frac{\pi}{2h} P - \frac{1}{C} \frac{\partial P}{\partial t} \quad (20)$$

For the reservoir upstream face radiation of acoustic waves, and

$$\rho \ddot{a}_{ns} = -\frac{\partial P}{\partial n} \quad (21)$$

For the interaction boundary between dam and reservoir.

In the above equations, z is the vertical coordinate, β is the acoustic impedance ratio of rock to water, n is the vector perpendicular to the boundary, ρ is the mass density of water, g is the gravitational acceleration, and \ddot{a}_{ns} is the absolute acceleration of dam upstream face in the normal direction. Here, we have assumed that the hydrodynamic waves satisfy the 1-D wave propagation Eq. (20), through the upstream reservoir near-field truncation surface. If we ignore the first term at right hand of Eq. (20), this boundary-sometimes known as the Sommerfeld or viscous boundary-performs well in time domain analysis when applied sufficiently far from the structure. The above equations along with the governing equation for the structure would lead to a simultaneous differential equations set for the coupled dam-reservoir system. These equations are discretized by the finite element method in a standard way similar to that of Ref (Ghaemian *et al.* 1998).

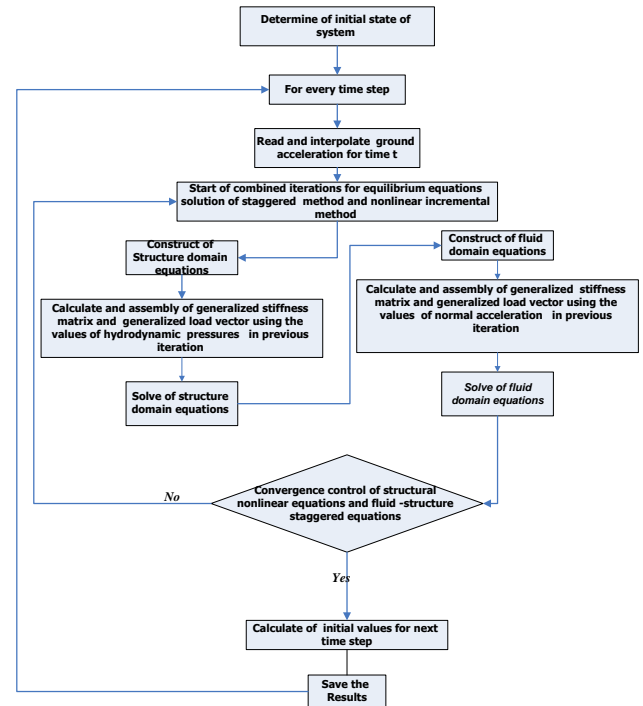


Fig. 3 The proposed staggered algorithm for fluid-structure interaction calculations

To avoid prohibitively high number of nonsymmetrical equations with a large bandwidth, the modified staggering solution method is employed (Moradloo 2007).

The implementation of the proposed staggered method is illustrated in Fig. 3 which shows all the operations needed to evaluate the necessary vectors and matrixes for fluid and structure domain, as well as needed iteration and criterion for terminating calculations. Here, the displacement and the pressure fields are solved alternatively in each time step to meet the “inter-domain compatibility” or convergence criteria (Fig. 3).

2.3 Computer implementation

The proposed models were implemented by finite element code GFEAP (Generalized Finite Element Code Program). GFEAP has capabilities of time history nonlinear dynamic analysis of arch dam, considering material, geometrical and construction joint nonlinearity and fluid structure interaction. It was prepared by writers for a complete nonlinear dynamic analysis of gravity and arch concrete dams, and it was developed based on the framework of FEAPPv program (Zienkiewicz and Taylor 2000)

2.4 Verification of models

The validity of the proposed models and numerical algorithms was checked using the available numerical results. Only one test is provided here. This model is a tension beam in which the ultimate load resistance is checked under direct displacement control approach in order to verify proposed smeared crack model. The three-

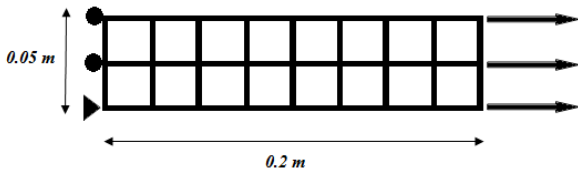


Fig. 4 Geometry and finite element mesh of the tension beam

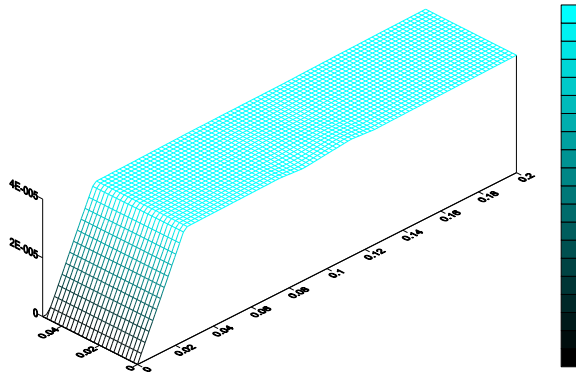


Fig. 5 Displacement distribution for prescribed displacement equal to 0.00004 m

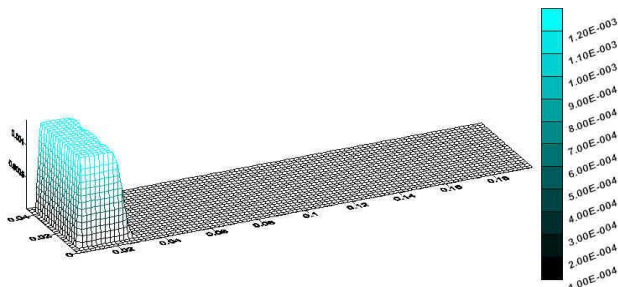


Fig. 6 Strain distribution for prescribed displacement equal to 0.00004 m

dimensional tension beam with unit thickness was tested under tension prescribed displacement (Fig. 4). The values used for material parameters module of elasticity, poisson ratio, tensile strength and the specific fracture energy were assumed as 20 GPa, 0, 2.0 MPa and 40 N/m, respectively. Strength of two elements near to supports was reduced for 5% to concentrate the fracture on these elements. The displacement and strain distributions are illustrated in Figs. 5 and 6, respectively. As shown in these figures, localization of strain and softening is evident in weakened elements. The displacement-load curve is presented in Fig. 7. As shown in these figures, the ultimate load is 95 KN (Fig. 7) which is equal to the analytical solution. The stress-strain curve of softened integration point is presented in Fig. 8. As shown in this figure, ultimate stress of weakened element (1.9 MPa) is precisely estimated. Moreover, softening behavior of concrete is precisely depicted. By calculating the area under the strain-stress curve and multiplying it by the characteristic length of the integration points (Eq. (14)), the value of specific fracture energy is calculated as 40 N/m which is equal to the actual value for the employed material. Moreover, based on the Eq. (15), the ultimate

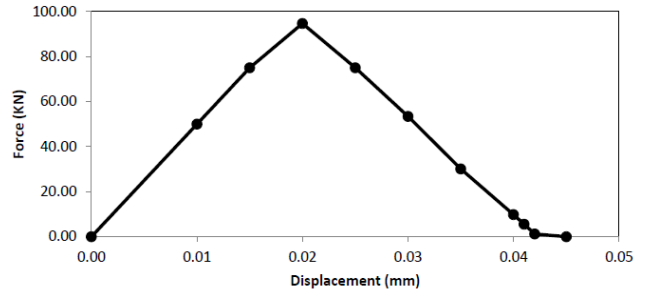


Fig. 7 Load-displacement curve for tension beam test

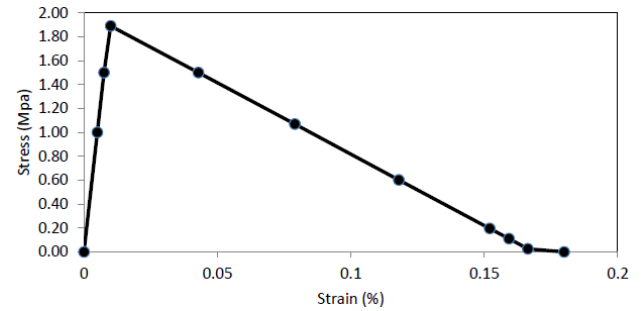


Fig. 8 Stress-strain curve of softened element

strain of concrete is estimated similar to ultimate strain in Fig. 8. Based on this figure, ultimate stress, crack initiation, fracture energy conservation and softening behavior are properly modeled.

4. Case study modeling, application on concrete arch dams

In this section, the nonlinear behavior of Karaj arch concrete dam is being studied by application of the models discussed above. The dam is 168 m high and the width of valley at crown elevation is 384 m on the Karaj River in Karaj, Iran. The thickness of the crown is 7.85 m and base of the dam is 32 m. This dam is an approximately symmetric, single-centered arch dam. Detailed geometry of this dam is provided in Mahab Gods (1990) and Rahimzadeh *et al.* (2003).

Fig. 9 shows the intended system which includes the finite element model of dam body and the reservoir in which the length of reservoir in the upstream direction is about two times the height of the dam. Moreover, the dam-foundation interaction is neglected. 1006 20-node solid elements and 7200 20-node fluid elements are used to model dam body and reservoir domain, respectively (Fig. 9). The modulus of elasticity, poisson ratio, density, compressive strength, tensile strength, fracture energy, dynamic magnification factors applied to tensile strength, modulus of elasticity, and fracture energy are 26GP, 0.17, 2450 kg/m³, 43 MPa 4.3 MPa, 260 Nm/m, 1.5, 1.25, and 1.8, respectively. The considered internal viscous damping ratio is 0.05 for the first and fifth vibration modes. The water level elevation for both hydrostatic and hydrodynamic pressure calculations is equal to the dam crest elevation (168 m). Acoustic wave velocity in water is *C*, 1440.0 m/s, and the acoustic impedance ratio of rock to

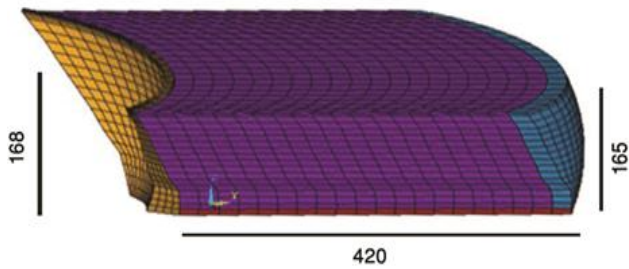


Fig. 9 Finite element model of reservoir and dam domain (dimensions are presented in meters)

water is $\beta=3.444$.

The loads applied on the system are self-weight, hydrostatic pressure and seismic load. The standard Newmark method is used to integrate dynamic equation into time domain. The Newmark parameters of α , β were assumed as 0.5, 0.25, respectively. The time integration steps were 0.01 and 0.005, alternatively. The Elasto -Brittle Damping (EDM) and Linear Damping model (LDM) have been used in dynamic analysis. The 14 points integration rule is used in elements volume numerical integration. It was found that this integration scheme compared to costume $3 \times 3 \times 3$ integration rule is more economical. The 8 selective ground motions are selected as the free-field ground acceleration (Figs. 10, 11 and Table 1). In Fig. 10, magnitude-distance diagram for selective acceleration gauges are presented. In Fig. 11, original components (without scale) of horizontal acceleration for three of considered events are presented as examples.

5. Fragility analysis

Fragility functions are the probability of reaching a defined structural limit under such loads as earthquake. More simply, a structural fragility curve describes the relation between ground seismic movement and the probable seismic damage. The correct selection of ground motions in dam site is required to determine the accurate relationship. The indexes which show the magnitude and intensity of ground motions in the fragility analysis are as follows: peak ground acceleration (PGA), peak ground velocity (PGV) and peak ground displacement (PGD). Fragility curves can be used to evaluate the probability of infrastructure failures. After determining the type of structural vulnerability, structural retrofit starts. To determine the seismic risk of a structure, it is essential to evaluate the severity of the damage during the earthquake with different scenarios. To generate fragility curves, based on time history analysis, the probabilistic methods are used. In this study, peak ground acceleration PGA is used. According to the PGA method, the structural fragility curves are defined in relation to structural limitations. Fragility analysis presents the probability of damage due to different earthquake records.

A fragility curve presents the corresponding damage probability regarding a particular mode of damage to in relation with different levels of seismic ground motion. The

seismic fragility curve of a structure describes the ratio between ground motion and the probable seismic damage level. Based on these curves, curves seismic reliability can be plotted that decreases the errors in interpreting the results of its fragility curve.

The structure fragility can be expressed mathematically as the damage probability of a structure in an earthquake with the magnitude of j and damage i , as represented in Eq. (22)

$$PF_{ij} = \text{Prob}[d_i \geq D_i / I_j] \quad (22)$$

Where PF_{ij} : fragility probability, ij : a certain amount of earthquake magnitudes for earthquake risk level, d_i : structural response due to these random events (e.g., drift of story in building), D_i : structural capacity to deal with the force at an i^{th} level of performance (e.g., life safety performance).

To produce fragility curves, a distribution for damage index should be obtained from nonlinear dynamic analyses. Usually normal, log normal and beta distributions are used. Normal distribution is one of the most important statistical distributions. This distribution diagram is known as the normal curve graph, the bell-shaped and more events that occur in nature and scientific research will follow this curve. Normal curve is also called the Gaussian distribution curve. A random variable X , with a bell-shaped distribution curve, is called a normal accidental variable. The distribution density function in Eq. (23) is as follows

$$f_x(X) = \frac{1}{\sigma\sqrt{2\pi}} e^{-\frac{1}{2}\left(\frac{x-\mu}{\sigma}\right)^2} \quad (23)$$

Where $f_x(X)$, n , μ and σ^2 are distribution function, number of data, mean and standard deviation, respectively

$$\mu = \frac{1}{n} \sum_{i=1}^n (x_i) \quad (24)$$

$$s^2 = \frac{1}{n-1} \sum_{i=1}^n (x_i - \bar{x})^2 \quad (25)$$

To calculate the probability of a normal distribution, the area of the normal curve called the normal cumulative distribution function is used. It can be obtained from Eqs. (26) and (27).

$$F_x(x) = f(x|\mu, \sigma) = \frac{1}{\sigma\sqrt{2\pi}} \int_0^x e^{-\frac{1}{2}\left(\frac{x-\mu}{\sigma}\right)^2} dx \quad (26)$$

$$F_x(x) = \frac{1}{\sigma\sqrt{2\pi}} \int_0^x e^{-\frac{1}{2}\left(\frac{x-\mu}{\sigma}\right)^2} dx = \Phi\left(\frac{x-\mu}{\sigma}\right) \quad (27)$$

Now if we desire to use the normal logarithmic distribution, a natural logarithm must be employed on all data and average and standard deviation must be obtained from the new data. Consequently, if we want to convert the normal logarithmic distribution into the normal distribution, we will have:

Log normal distribution $(x, \mu, \sigma) = \text{Normal distribution} (\ln(x) - \mu/\sigma)$

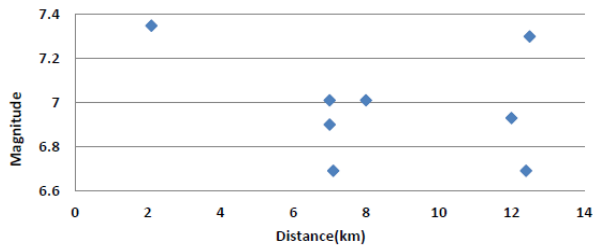


Fig. 10 Magnitude-distance diagram for selective acceleration

Table 1 Selective records used in nonlinear seismic analysis

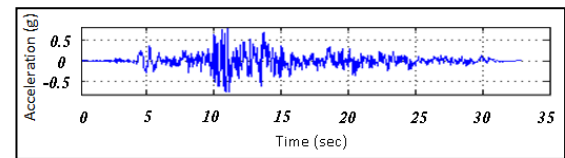
Earthquake	Station	Year	Magnitude	R(km)	V _{s30} m/s
Kobe	Nishi Akashi	1995	6.9	7	610
Manjil	Abbar	1990	7.3	12.5	724
Cape Mendocino	Petrolia	1992	7.01	8	712
Northridge-01	Pacoima Dam	1994	6.69	7.1	2016
Tabas	Tabas	1978	7.35	2.1	766
Loma Prieta	Observatory	1989	6.93	12	714
Northridge-01	Hills 12250	1994	6.69	12.4	545
Cape Mendocino	Cape Mendocino	1992	7.01	7	513

Table 2 Natural frequency of dam in empty and full reservoir condition

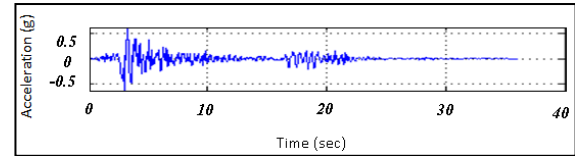
Reservoir Condition	Mode Number										
		1	2	3	4	5	6	7	8	9	10
Empty reservoir	Current Analysis	2.22	2.63	3.69	4.7	4.86	5.61	6.11	7.6	7.78	8.23
	Mahab Gods (1990) and Rahimzadeh <i>et al.</i> (2003)	2.18	2.78	3.59	4.45	4.97	5.83	5.91	7.62	7.94	8.23
Full reservoir	Current Analysis	1.88	2.23	2.59	3.09	3.43	4.02	4.7	4.88	5.08	5.54
	Mahab Gods (1990) and Rahimzadeh <i>et al.</i> (2003)	1.86	2.3	2.67	2.93	3.32	4.04	4.13	4.59	5	5.42

5.1 Sampling by a time history nonlinear analysis

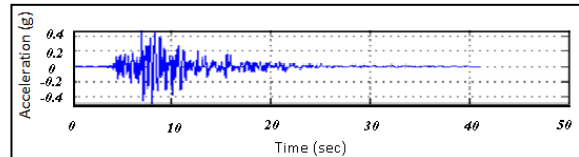
To select earthquake records, in addition to soil features of the site, such factors as the type of earthquake domain, record duration and seismic risks should be considered. Because Karaj dam is located on a coarse-grained diorite, an igneous rock without weathering, its foundation is a stable rock mass according to rock mechanics. According to Iran seismic design code, the dam soil type is very stiff and is type (I). Since the northwest fault of Tehran is near to the dam site, near field records of various earthquakes are considered in the analysis. Such parameters as Arias intensity, damage potential, total cumulative velocity and the distance from the fault are factors which are important in defining the field records (Hajhoseyni and Moradloo 2014). In addition to the factors mentioned above, the frequency of content and pulse-like motions are effective in near field records. According to the above criteria, eight earthquake records were selected (Hajhoseyni and Moradloo 2014). The records contents are shown in Table 1.



A: Tabas earthquake



B: Northridge-01(Pacoima Dam) earthquake



C: Kobe (Nishi Akashi) earthquake

Fig. 11 Time history of horizontal acceleration components without scale

Table 3 PGA values for Amirkabir dam site for MCE and DBE (Mahab Gods 1990 and Rahimzadeh *et al.* 2003)

Design level	Period (year)	PGA	
		Horizontal	Vertical
DBE (Design Basis Earthquake)	100-1000	0.23 g	0.16 g
MCE (Maximum Credible Earthquake)	>3000	0.43 g	0.33 g

Fig. 10 represents the magnitude-distance diagram for selective accelograms. As shown in Fig. 10 and Table 1, the focal distance of the considered earthquake records is less than 13 km and their magnitude ranges from 6.69 to 7.35 Richter.

In order to verify the model, the modal frequency of the dam was calculated and compared to the results of references (Mahab Gods 1990 and Rahimzadeh *et al.* 2003). The natural frequencies of dam body alone and dam reservoir system are shown in Table 2. The obtained results (Table 2) are consistent with the results in references. To evaluate the seismic vulnerability of Karaj arch dam, 8 near-field records, all scaled between 0.2 g to 0.8 g, were used. For each record seven nonlinear analyses with 0.1 g intervals were performed. Some of the horizontal components of used acceleration records are presented in Fig. 11. The other earthquake characteristics are presented in Table 1. The Raylight damping model was used in nonlinear dynamic analysis with 5% critical damping ratio taking one and third modes into account.

PGA values for Karaj dam site for Maximum Credible Earthquake (MCE) and Design Basis Earthquake (DBE) are presented in Table 3 (Mahab Gods 1990 and Rahimzadeh *et al.* 2003). Since three dimensional analysis of the dam is performed, the value of horizontal PGA in transverse direction is used again. In order to use the fragility curve, the square roots of sum of square of three PGA in vertical, stream line and transverse of river should be considered as a

Table 4 Volume of damaged concrete for selective records versus PGA values (in cubic meters)

Considered Earthquake	Part of Dam Body	Scale of Record							
		0.2 g	0.3 g	0.4 g	0.5 g	0.6 g	0.7 g	0.8 g	
Kobe	Dam body	8265	11450	17305	24185	54265	118613	231945	
	Crown part	0	0	0	0	3040	8087	14013	
	Total	8265	11450	17305	24185	57305	126700	245958	
Northridge-01 (Pacoima)	Dam body	6255	9518	12275	16828	18071	25916	39490	
	Crown part	0	0	0	0	0	0	450	
	Total	6255	9518	12275	16828	18071	25916	39940	
Cape Mendocino (Pretoria)	Dam body	8588	11890	16065	24679	57089	110973	229238	
	Crown part	0	0	0	148	3692	6415	9791	
	Total	8588	11890	16065	24827	60781	117388	239029	
Tabas	Dam body	5896	9785	13346	18744	29017	71089	177337	
	Crown part	0	0	0	0	0	5075	10229	
	Total	5896	9785	13346	18744	29017	76163	187566	
Loma Prieta	Dam body	4625	6330	8983	11804	14920	21120	31025	
	Crown part	0	0	0	0	0	0	380	
	Total	4625	6330	8983	11804	14920	21120	31405	
Northridge-01 (Hills)	Dam body	4670	8050	11392	16926	23900	35237	61954	
	Crown part	0	0	0	0	0	85	2710	
	Total	4670	8050	11392	16926	23900	35322	64664	
Cape Mendocino (Cape Mendocino)	Dam body	4220	8120	9993	12135	15020	17068	17670	
	Crown part	0	0	0	0	0	0	0	
	Total	4220	8120	9993	12135	15020	17068	17670	
Manjil	Dam body	5156	8950	11750	15131	17632	23155	28590	
	Crown part	0	0	0	0	0	0	0	
	Total	5156	8950	11750	15131	17632	23155	28590	

Table 5 Minimum and maximum displacement of dam crown for selective records versus PGA values

Records	PGA	0.2 g	0.3 g	0.4 g	0.5 g	0.6 g	0.7 g	0.8 g
		max	-1	0.5	2.1	3.65	6.15	10.85
min	-7.60	-9.30	-11.20	-13.00	-14.65	-16.65	-19.04	
Pacoima	max	-1.60	0.00	0.70	2.00	3.10	4.30	5.35
	min	-6.40	-7.50	-8.60	-9.90	-11.00	-12.10	-13.20
Pretoria	max	-0.50	1.20	3.05	5.00	7.60	11.60	15.8
	min	-7.20	-8.80	-10.40	-12.01	-13.90	-16.70	-20.70
Tabas	max	-1.30	0.20	1.60	3.13	4.60	7.30	11.54
	min	-7.30	-9.02	-10.75	-12.50	-14.00	-15.60	-17.20
Loma	max	-2.30	-1.40	-0.50	0.50	1.30	2.20	3.01
	min	-5.90	-6.80	-7.80	-8.70	-9.70	-10.60	-11.58
Hills	max	-1.90	-0.70	0.50	1.55	2.65	3.70	4.72
	min	-6.80	-8.30	-9.70	-11.00	-12.20	-13.30	-14.44
Cape cape	max	-3.10	-2.60	-2.05	-1.60	-1.03	-0.50	0.5
	min	-5.30	-6.05	-6.75	-7.35	-8.05	-8.75	-9.45
Manjil	max	-2.20	-1.15	0.00	0.80	1.80	2.80	3.81
	min	-6.45	-7.75	-9.00	-10.20	-11.50	-12.75	-14.04

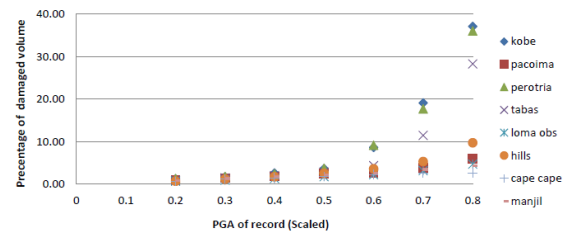


Fig. 12 Percentage of damaged concrete volume for selective records versus PGA values

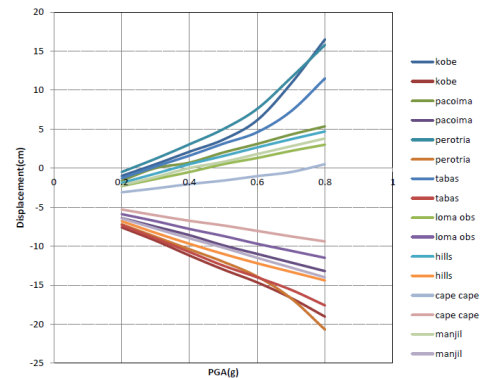


Fig. 13 Minimum and maximum displacement of dam crown for selective records versus PGA values

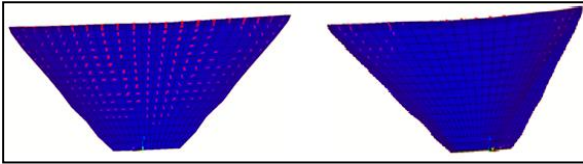


Fig. 14 Crack distribution at upstream and downstream of the dam for Tabas earthquake loading (1.2 g)

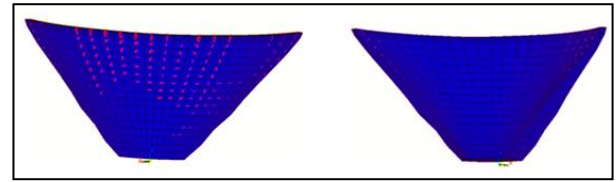


Fig. 16 Crack distribution at upstream and downstream of the dam for Kobe earthquake loading (0.8 g)

Table 6 Volume of damaged concrete and crown displacement to determine the limit state values

Earthquakes	PGA (g)	Crown displacement (cm)	Damaged concrete volume (m ³)
Kobe	0.8	19.5	245900
Cape (Petrolia)	1	29	450050
Tabas	1.2	38.2	502000

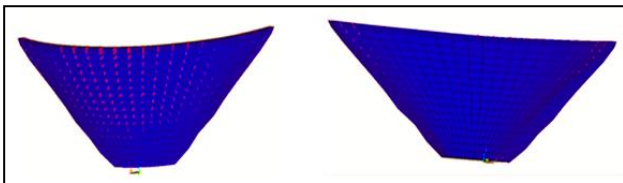


Fig. 15 Crack distribution at upstream and downstream of the dam for Cape earthquake loading (1 g)

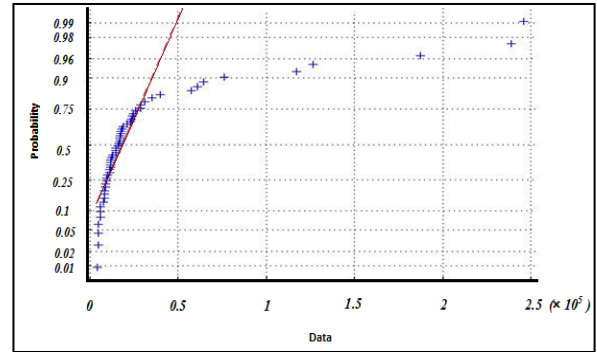


Fig. 17 Results using normal distribution

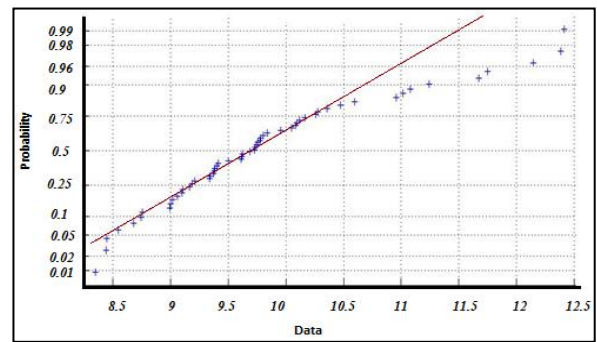


Fig. 18 Results using log normal distribution

single measure. The resultant values for DBE and MCE are 0.36 g and 0.69 g, respectively.

The volumes of damaged concrete for selective records versus PGA values are presented in Table 4 and Fig. 12. Moreover, the minimum and maximum displacements of dam crown for selective records versus PGA values are presented in Table 5 and Fig. 13.

5.2 Limit states and damage index

According to the regulations and laboratory research on frames and bridges, the choice of appropriate performance levels for such structures is not very difficult. However, the inaccessibility of enough laboratory results and statutory regulations has caused the engineering judgment play an influential role in determining the damage indexes and limit states for concrete dams.

As performance of concrete arch dams is completely different from gravity concrete ones, different indexes should also be considered here. Considering such factors as sliding between the dam and its foundation and dam body overturning are not suitable for arch concrete dam. Since the model is a three-dimensional model, cracked concrete volume in the dam body and crest displacement relative to rigid foundation can be suitable damage indexes. Of course, stability of arch dams is highly dependent on its foundation stability which its failure, displacement and sliding can be used as suitable damage indexes. In this research the foundation of the dam is assumed to be rigid, so the dam foundation criteria will be subject to further investigation.

To evaluate the seismic vulnerability of Karaj arch dam, 8 near-field records which all were scaled between 0.2 g to

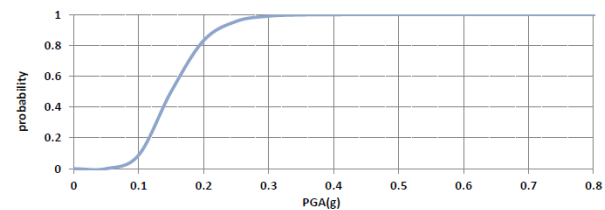


Fig. 19 Seismic fragility for displacement damage (LS1-l: low damage limit state)

0.8 g are used. For each record seven nonlinear analyzes with 0.1 g intervals were performed.

This accelograms scaled step by step with an interval of 0.1 g and then the dam-reservoir system was loaded until the dam was completely destroyed and system diverged. The results for concrete damage and dam crown displacement for each record are shown in Table 6. The distribution of these cracks for the ultimate state are shown in Figs. 14, 15 and 16 for Tabas, Cape and Kobe earthquakes, respectively. The values of damaged volume are used to determine the limit state values. Damaged concrete volume and crown displacement results for determining the limit state values are presented in Table 6. The limit states are selected as follows: 50% of the ultimate

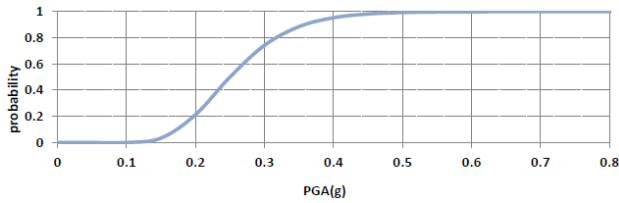


Fig. 20 Seismic fragility for displacement damage (LS1-m medium damage limit state)

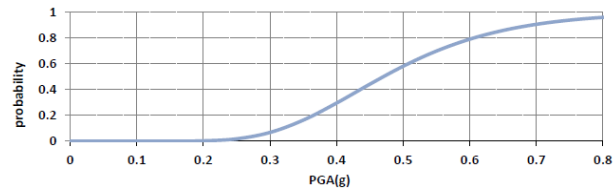


Fig. 21 Seismic fragility for displacement damage (LS1-e extreme damage limit state)

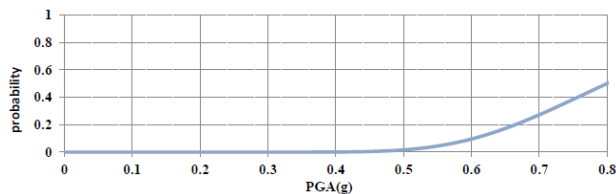


Fig. 22 Seismic fragility for displacement damage (LS1-c complete damage limit state)

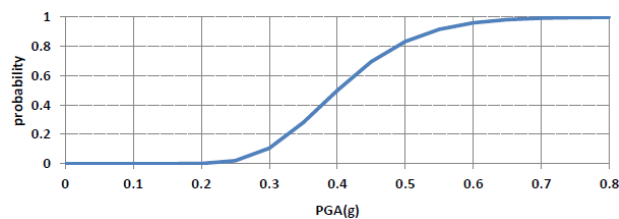


Fig. 23 Seismic fragility for cracking damage (LS2-l low damage limit state)

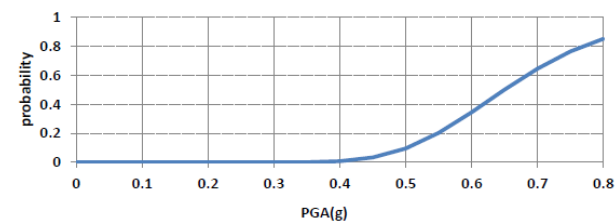


Fig. 24 Seismic fragility for cracking damage (LS2-m medium damage limit state)

minimum damage is called complete destruction, 40% is called extreme destruction, 20% is called medium destruction and 10% is called low destruction.

5.3 Fragility curves

The results obtained from the nonlinear analysis are employed to obtain the log normal and normal statistical distribution. In Figs. 17 and 18, results are presented using normal and log-normal distributions, respectively. According to Figs. 17 and 18, it is evident that the results

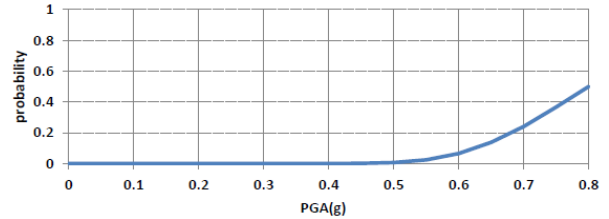


Fig. 25 Seismic fragility for cracking damage (LS2-e extreme damage limit state)

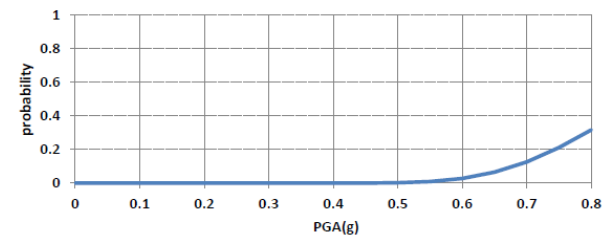


Fig. 26 Seismic fragility for cracking damage (LS2-c complete damage limit state)

Table 7 Summary of seismic fragilities results obtained from a nonlinear analysis

Limit State (LS)		Nonlinear Results	
		Prob of LS at PGA= 0.36 g	Prob of LS at PGA= 0.69 g
LS1-l	Low crown displacement	100%	100%
LS1-m	medium crown displacement	90%	100%
LS1-e	extreme crown displacement	20%	9%
LS1-c	complete crown displacement	0%	28%
LS2-l	low tensile cracked Elements	20%	100%
LS2-m	medium tensile cracked elements	0%	60%
LS2-e	extreme tensile cracked elements	0%	25%
LS2-c	complete tensile cracked elements	0%	14%

more homogeneously fit the lognormal distribution. So, the probability distribution function of the log normal was used to extract the fragility curves.

According to defined performance levels, using the log-normal distribution, as well as results of the dynamic nonlinear time history analysis, we draw fragility curves. The Step by step fragility curves drawing are as follows:

1. The necessary data for each PGA is obtained from nonlinear analysis.

2. The average and standard deviation of data is calculated for each PGA.

3. According to the statistical distribution, lognormal distribution in this study, the probability of exceeding the limitations is calculated.

The fragility curves are presented according to the method mentioned above.

After obtaining the fragility curves, the probability of a given structural limitation is defined. One of features of this method is that by evaluating earthquakes with different

characteristics, decisions can be made about the safety, the probability of reaching a structural limit, strengthening and rehabilitation of a structure. In the other methods, you need to apply a lot of different earthquake records on structures. However, the complete structural behavior of each earthquake is not obtained finally. Since each earthquake is different from others and even in the same earthquake the soil type and distance can incur different degrees of structural damage, the earthquake modeling without proper statistical methods will not yield meaningful results in many instances. With the fragility curves, the probability of exceeding the structural limit can be easily calculated. Figs. 19 to 22 represent the fragility curves of the crown displacement damage index for all 4 limit states. Furthermore, in Figs. 23 to 26, the fragility curves of the cracking damage index for all 4 limit states are presented.

For a DBE earthquake level with a PGA of 0.23 g, it can be seen that the probability of the first structural limit i.e. crest displacement for low, medium, extreme and complete damage limit states are 0, 0, 40 and 100, respectively. For the MCE level, these amounts are 0, 40, 100 and 100, respectively.

The results of seismic fragilities obtained from nonlinear analysis are summarized in Table 7. Since the dam is designed for an earthquake with a 300-years return period, it can be seen that the dam shows a high resistance against earthquakes at DBE level which is only damaged in low function levels. By evaluating the effects of damage indexes on fragility curves it can be understood that there is a wide range of differences in the curve results, and for a 0.36 g structural record the displacement damage index reaches to 100%. But for the cracked damage index, this value is 20%. Also, for higher function levels (extreme damage) as the PGA amount increases, the damage probability percentage of the two indexes becomes nearer to each other. It seems that the displacement index is more a conservative and impractical index in the fragility analysis.

6. Conclusions

This study presents a method to study fragilities of arch concrete dams and to assess their performance against seismic hazards. Firstly, the probability risk and fragility curves are presented. Then, in order to implement and demonstrate the usage of this method, some non-linear dynamic analyses are conducted on Amirkabir arch concrete dam (Karaj dam in Iran). The analysis takes the complete dynamic interaction of fluid and structure into consideration. The foundation is assumed as rigid.

The non-linear behavior of dam concrete material in analysis is modeled according to the smeared crack model. A modified three dimensional smeared crack model is used to consider nonlinear behavior of mass concrete. The proposed model considers major characteristics of mass concrete fewer than three dimensional loading conditions. These characteristics are pre-softening behavior, softening initiation criteria, fracture energy conservation and strain rate effect. Results show that the proposed crack model is high-performance and stable. In the present analysis,

complete fluid-structure interaction is considered accounting for fluid compressibility and absorptive reservoir boundary condition appropriately.

Based on the analysis results, fragility curves are obtained according to various and probable damages. Two damage indexes were introduced and compared to one another. The results indicate that the dam has a proper stability for earthquakes at DBE level. And for MCE earthquake events, the dam retains its stability. Of course, extensive cracking can take place in the dam body which needs to be rehabilitated. Moreover, displacement damages index is more conservative and impractical in the fragility analysis than tensional damage index.

References

- Alembagheri, M. and Ghaemian, M. (2013), "Damage assessment of a concrete arch dam through nonlinear incremental dynamic analysis", *Soil Dyn. Earthq. Eng.*, **44**, 127-137.
- Al-Eidi, B. and Hall, J.F. (1989a), "Non-linear earthquake response of concrete gravity dam, Part 1: Modeling", *Earthq. Eng. Struct. Dyn.*, **18**(6), 837-851.
- Al-Eidi, B. and Hall, J.F. (1989b), "Non-linear earthquake response of concrete gravity dam, Part 2: Behavior", *Earthq. Eng. Struct. Dyn.*, **18**(6), 85-865.
- Battacharjee, S. and Leger, P. (1992), "Concrete constitutive model for non-linear seismic analysis of gravity dams state-of-the-art", *Can. J. Civil Eng.*, **19**(3), 492-509.
- Borekci, M. and Kircil, M.S. (2011), "Fragility analysis of R/C frame buildings based on different types of hysteretic model", *Struct. Eng. Mech.*, **39**(6), 795-812.
- Dechun, L., Xiuli, D., Guosheng, W., Annan, Z. and Anke, L. (2016), "A three-dimensional elastoplastic constitutive model for concrete", *Comput. Struct.*, **163**, 41-55.
- Ellingwood, B.R. and Tekie, P.B. (2001), "Fragility analysis of concrete gravity dams", *J. Infrastruct. Syst.*, **7**(2), 41-48.
- Faria, R., Oliver, J. and Cevera, M. (1998), "A strain-based plastic viscose damage model for massive concrete structures", *Int. J. Sol. Struct.*, **35**(14), 1533-1558.
- Feng, L.M and Pekauo, O.A. (1996), "Cracking analysis of arch dams by 3D boundary element method", *J. Struct. Eng.*, **122**(6), 691-699.
- Ghaemian, M. and Ghobarah, A. (1998), "Staggered solution schemes for dam-reservoir interaction", *J. Flu. Struct.*, **12**(7), 933-948.
- Ghaemian, M. and MirzahasseinKashani, S. (2009), "Seismic fragility assessment of concrete gravity dams", *Proceedings of the 29th USSD Annual Meeting and Conference on Managing our Water Retention Systems*, Nashville, Tennessee, April.
- Ghrib, F. and Tinawi, R. (1995), "An application of damage mechanics for seismic analysis of concrete gravity dams", *Earthq. Eng. Struct. Dyn.*, **24**(2), 157-173.
- Gunglun, W., Pekau, O.A., Chuhan, Z. and Shaumin, W. (2000), "Seismic fracture analysis of concrete gravity dams based on nonlinear fracture mechanics", *Eng. Fract. Mech.*, **65**(1), 67-87.
- Hajhoseyni, J. and Moradloo, J. (2014), "Comparison of near-field and far-field earthquake on nonlinear response of concrete gravity dams", *J. Civil Environ. Eng.*, **44**(4), 42-52.
- Hariri-Ardebili, M.A., Seyed-Kolbadi, S.M. and Mirzaboz, H. (2013), "A smeared crack model for seismic failure analysis of concrete gravity dams considering fracture energy effects", *Struct. Eng. Mech.*, **48**(1), 17-39.
- Hariri-Ardebili, M.A. and Saouma, V.E. (2016), "Probabilistic seismic demand model and optimal intensity measure for

- concrete dams”, *Struct. Safety*, **59**, 67-85.
- Jovanoska, E.D. (2000), “Fragility curves for reinforced concrete structures in Skopje (Macedonia) region”, *Soil Dyn. Earthq. Eng.*, **19**(6), 455-466.
- Kadkhodayana, V., Aghajanzadehb, M. and Mirzabozorg, H. (2015), “Seismic assessment of arch dams using fragility curves”, *Civil Eng. J.*, **1**(2), 14-20.
- Karim, K.R. and Yamazaki, F. (2001), “Effect of earthquake ground motions on fragility curves of highway bridge piers based on numerical simulation”, *Earthq. Eng. Struct. Dyn.*, **30**(12), 1839-1856.
- Kang, J.W. and Lee, J. (2016), “A new damage index for seismic FRAGILITY analysis of reinforced concrete columns”, *Struct. Eng. Mech.*, **60**(5), 875-890.
- Lan, L. and John, A. (2008), “Seismic bulnerability and prioritization ranking of dams in Canada”, *Proceedings of the 14th World Conference on Earthquake Engineering*, Beijing, China, October.
- Mahab Gods Consulting Engineering Co. (1990), *Data Book of Karaj Concrete Arch Dam*.
- Mehan, Y., Bechtoula, H., Kibboua, A. and Naili, M. (2013), “Assessment of seismic FRAGILITY curves for existing RC buildings in Algiers after the 2003 Boumerdes earthquake”, *Struct. Eng. Mech.*, **46**(6), 791-808.
- Mirzabozorg, G. (2004), “Damage mechanics approach in seismic analysis of concrete gravity dams including dam-reservoir interaction”, *Eur. Earthq. Eng.*, **18**(3), 17-24.
- Mirzabozorg, G. and Ghaemian, M. (2005), “Non-Linear behavior of mass concrete in three-dimensional problems using a smeared crack approach”, *Earthq. Eng. Struct. Dyn.*, **34**(3), 247-269.
- Moradloo, J. (2007), “Nonlinear dynamic analysis of arch concrete dam considering large displacements”, Ph.D. Dissertation, Department of Civil Engineering, TMU.
- Omidi, O., Valliappan, S. and Lotf, V. (2013), “Seismic cracking of concrete gravity dams by plastic-damage model using different damping mechanisms”, *Fin. Elem. Analy. Des.*, **63**, 80-97.
- Oudni, N. and Bouafia, Y. (2015), “Response of concrete gravity dam by damage model under seismic excitation”, *Eng. Fail. Anal.*, **58**, 417-428.
- Pekau, O.A., Chuhan, Z. and Lingmin, F. (1995), “Seismic fracture of koyna dam: Case study”, *Earthq. Eng. Struct. Dyn.*, **24**(1), 15-33.
- Rahimzadeh, F. and Omodi, O. (2003), *Investigating of Concrete Nonlinearity of Seismic Response of Concrete Arch Dam*, Research Report, Water Resources Management Co. (WRMC).
- Shinozuka, M., Banerjee, S. and Kim, S.H. (2007), *Fragility Considerations in Highway Bridge Design*, MCEER, MCEER-07-0023, 192.
- Zienkiewicz, O.C. and Taylor, R.L. (2000), *The Finite Element Method, Solid Mechanics*, Butterworth Heinmann.